Figure 7.1

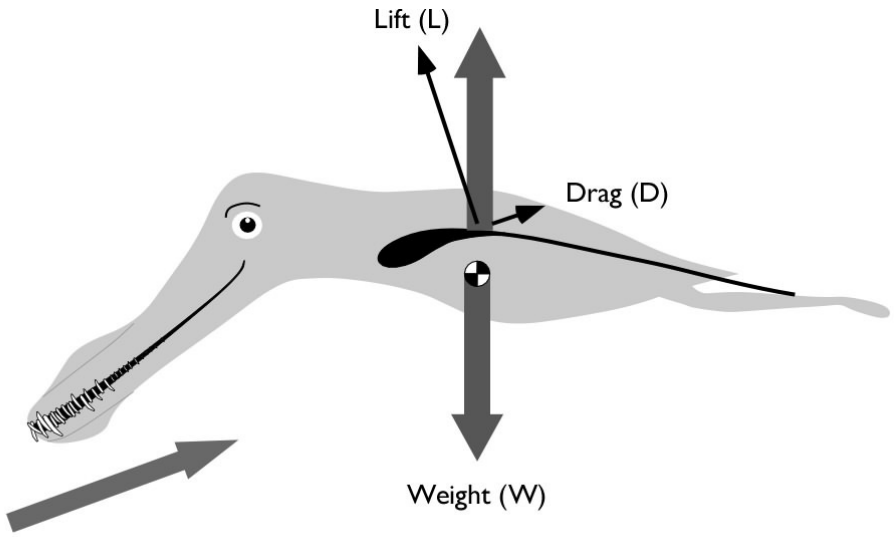

Forces in steady flight. The resultant of lift and drag must be exactly equal to the weight, and act in the opposite direction, with the lines of action being coincident.

Figure 7.2

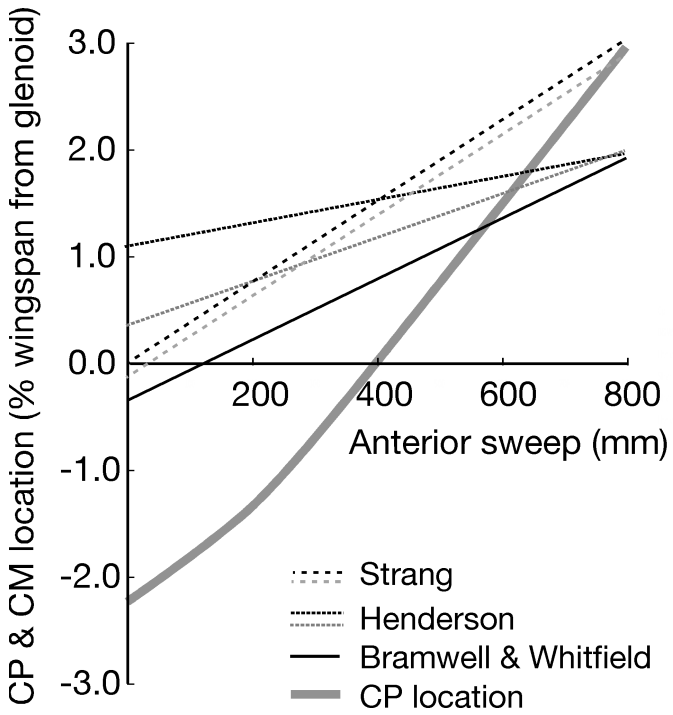

Variation of Centre of Pressure (CP) and Centre of Mass (CM). The thick grey line is the movement of the aerodynamic CP with increasing anterior sweep. The thinner lines are the movement of the CM under different reconstruction assumptions. In all cases balance (coincidence of CM and CP) is only achieved with substantial anterior sweep (at least 600mm).

Figure 7.3

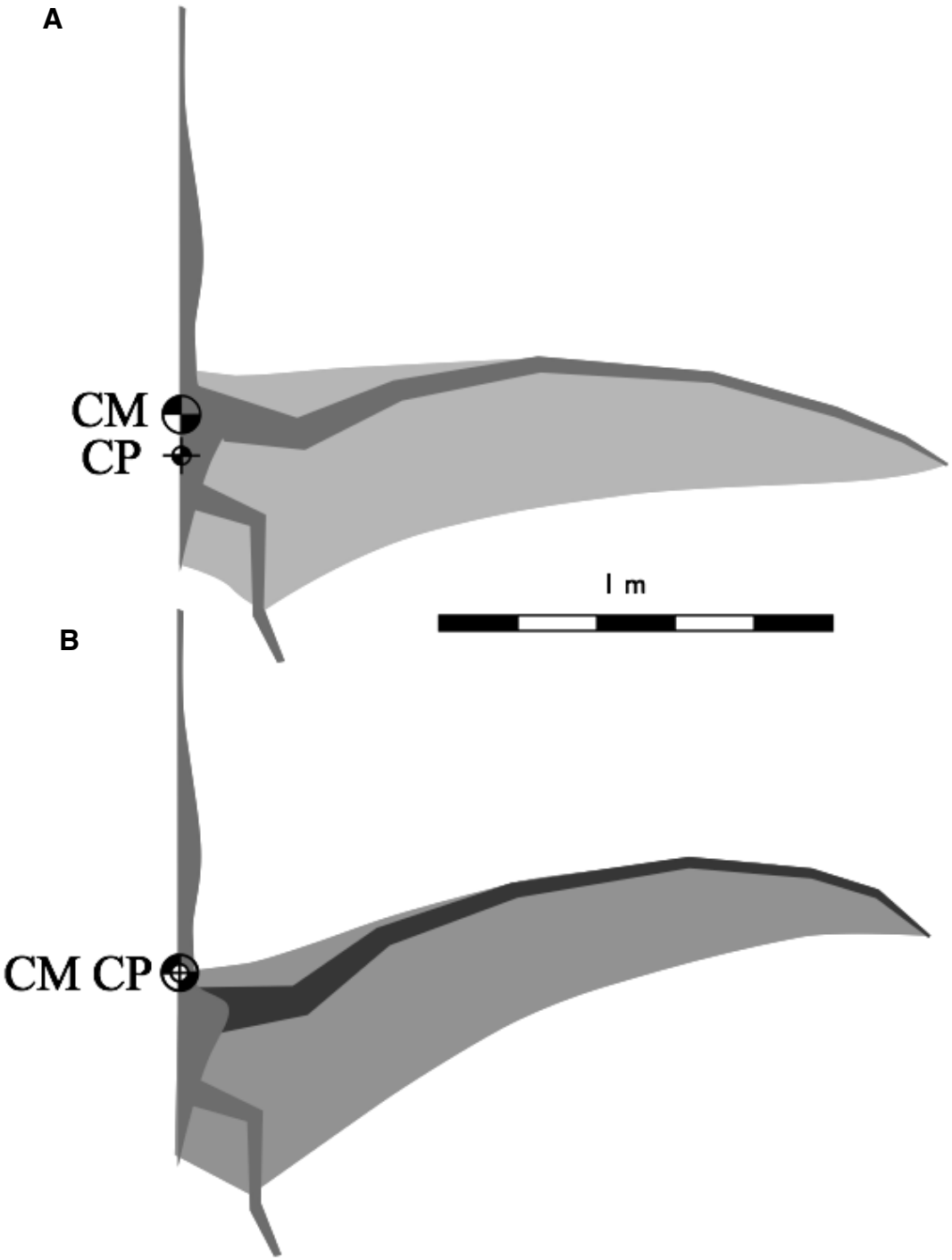

Pteraondon wing shape. (A) a typical morphology as found in the literature (e.g. Henderson 2010), showing the centres of mass and pressure are not coincident. The CM is near the base of the neck and the CP posterior to the glenoid. In (B), the wing has been swept anteriorly until the CM and CP are coincident.

Figure 7.4

Selected membrane structures subject to aerodynamic forces. (A)

Windsurfer sail with convex free margin supported by battens in compression against the mast. The sail has a strip of high tensile material along the posterior edge to apply compression to the battens and maintain the tension in the sail material between the battens. (B) Hang glider with similar stiffening battens and trailing edge "tendon". (C) Large fruit bat, showing how the fingers serve to support the wing membrane, but due to the lack of a trailing edge tendon, the free margins between the fingers is markedly convex. A similar shape is seen in the stunt kite (D) and the sails of a South Indian fishing boats (E). The banner (F) has a convex free margin but being unsupported by any in-plane tension, consequently it simply flaps in the wind.

Figure 7.5

Typical input screen for XFLR5. The upper left panel is the wing geometry definition, describing both the wing outline and local wing section. The right hand panel lists the overall characteristics and dimensions.

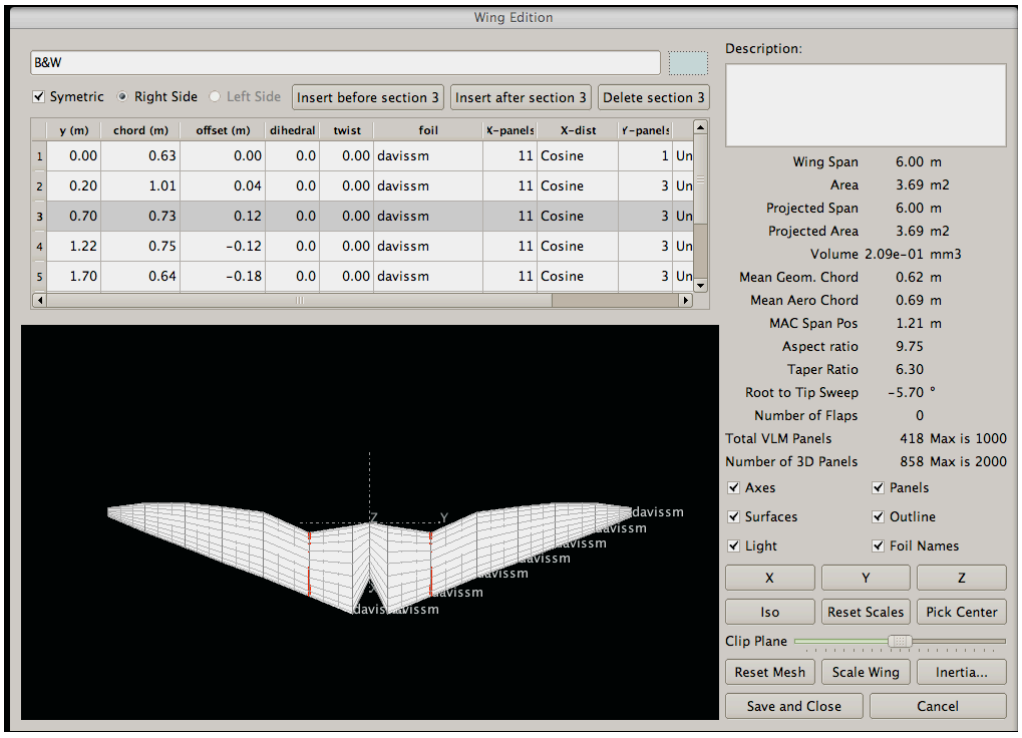

Figure 7.6

XFLR5 output screen showing pressure distribution over a wing (coloured contours) and stream lines in the wake.

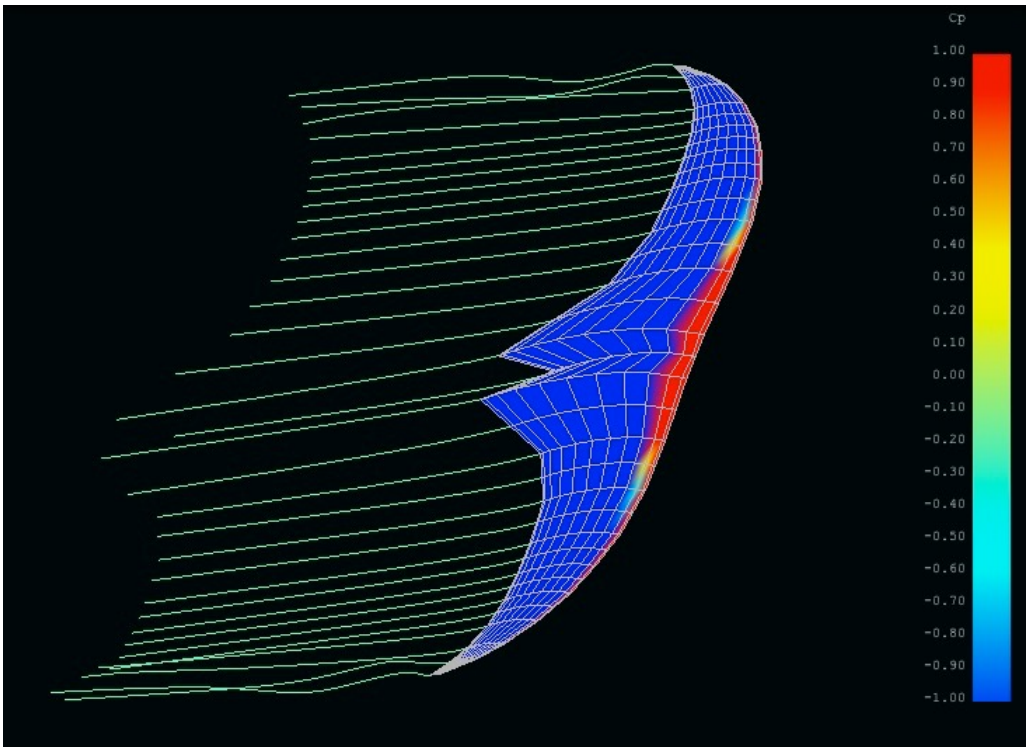

Figure 7.7

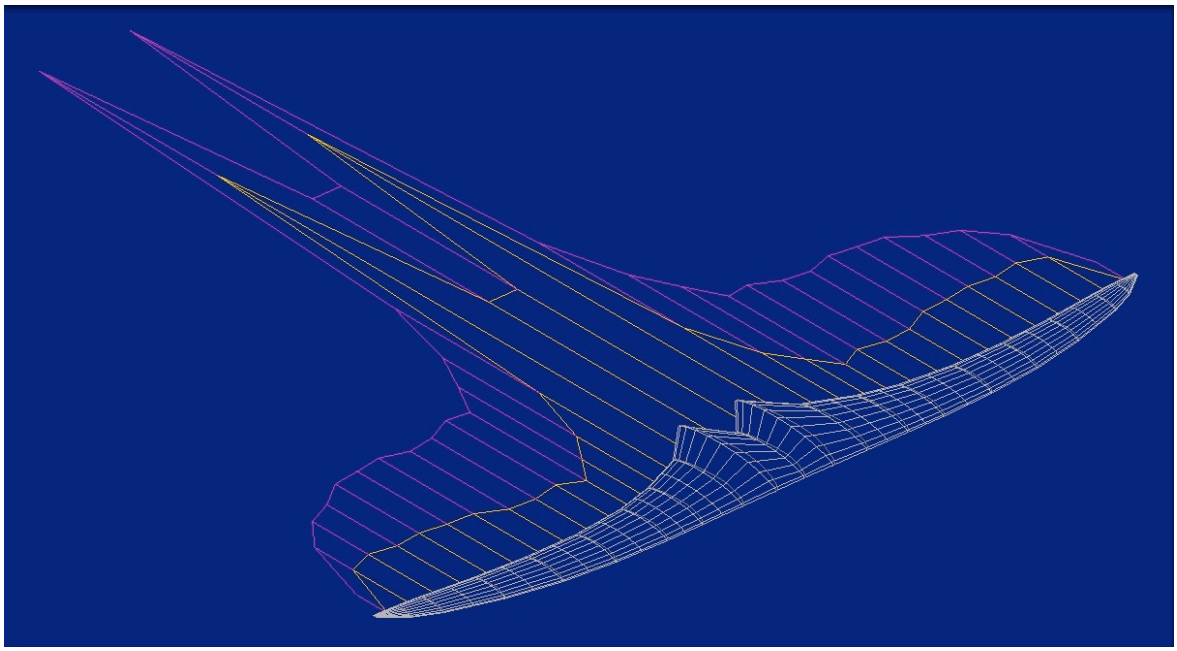

XFLR5 output screen showing spanwise variation of induced drag (yellow lines) and total drag (blue lines).

Figure 7.8

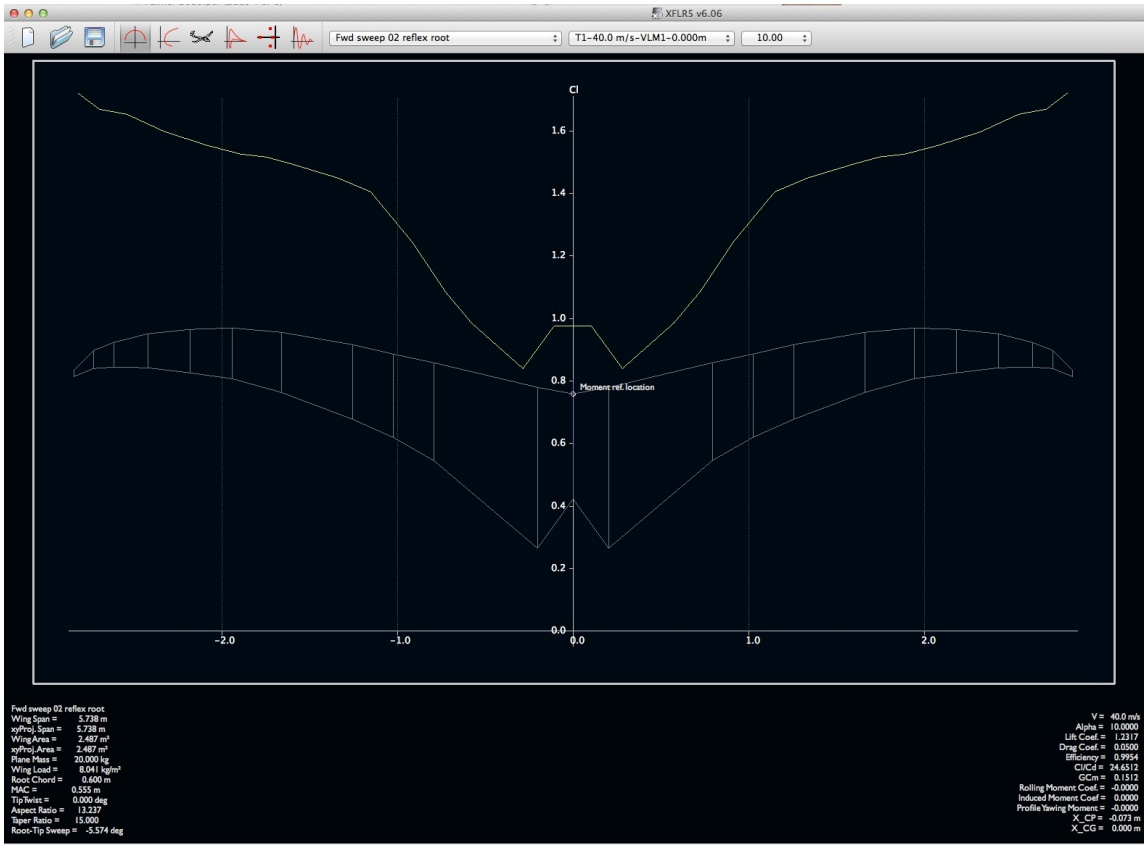

XFLR5 output screen showing spanwise variation of lift coefficient at one specific angle of attack.

Figure 7.9

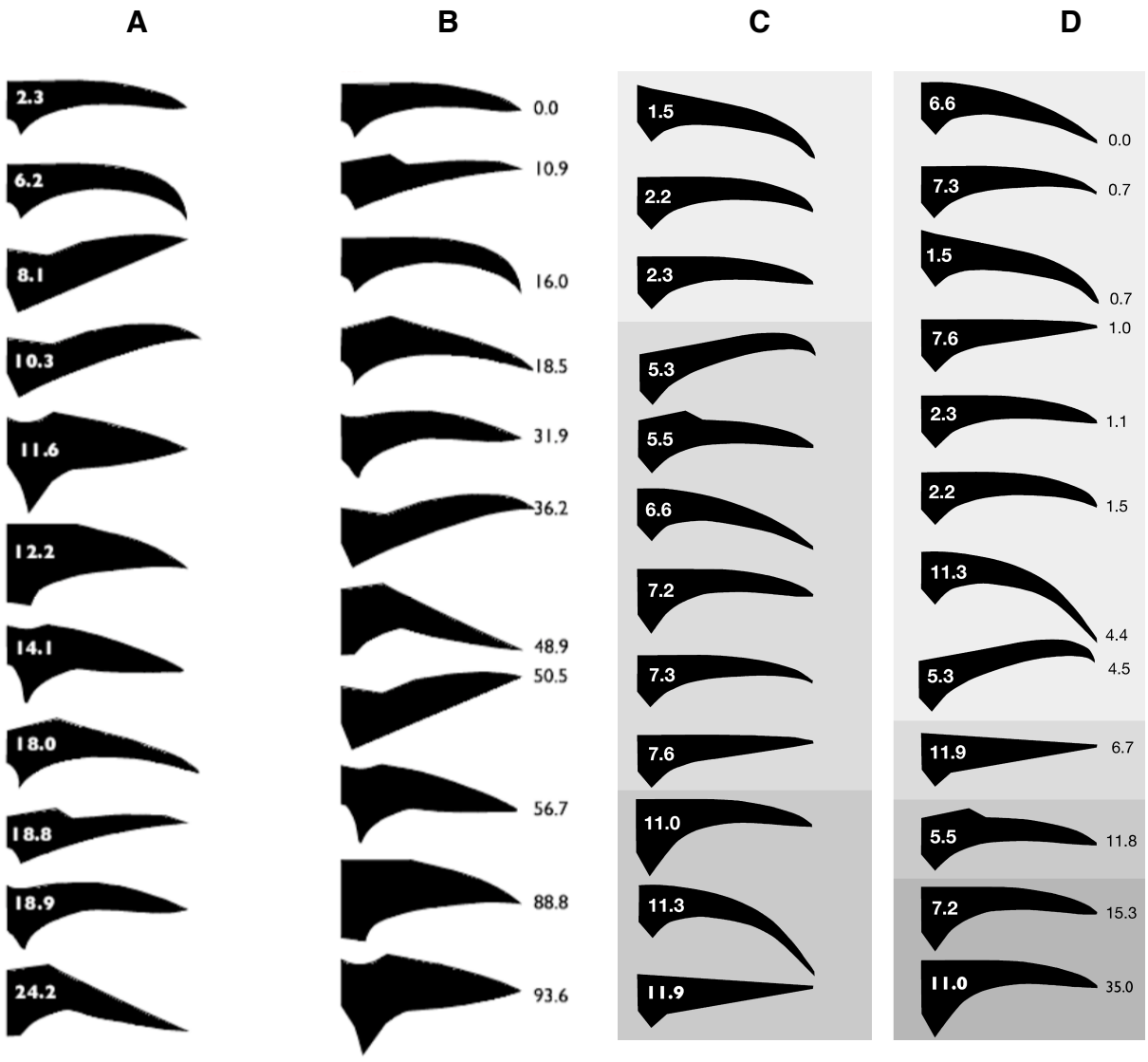

Range of wing shapes investigated using XFLR5. (A) and (B): shapes from Bramwell & Whitfield (1974), Bennett (2007), Wilkinson (2008), Witton (2009) and Unwin (2005). They are presented in descending order of aspect ratio. (C) and (D): a set of variations derived from Bennett (2007). All of very similar aspect ratio, but differing in taper, sweep, wing bone curvature and body length.

The relative performance of the different shapes is compared in two ways. First (A) and (C) the induced drag was compared with the induced drag of an ideal elliptical wing of the same aspect ratio, to yield a ratio related to the well known span efficiency ‘e’. The shapes were also compared on the basis of a direct comparison of induced drag coefficient (B) and (D).

Figure 7.10

A B

Example of comparison of XFLR5 results for different planforms. (A) spanwise variation of induced drag coefficient, (B) local angle of attack, (C) local lift coefficient and (D) local lift. Two pterosaur wing

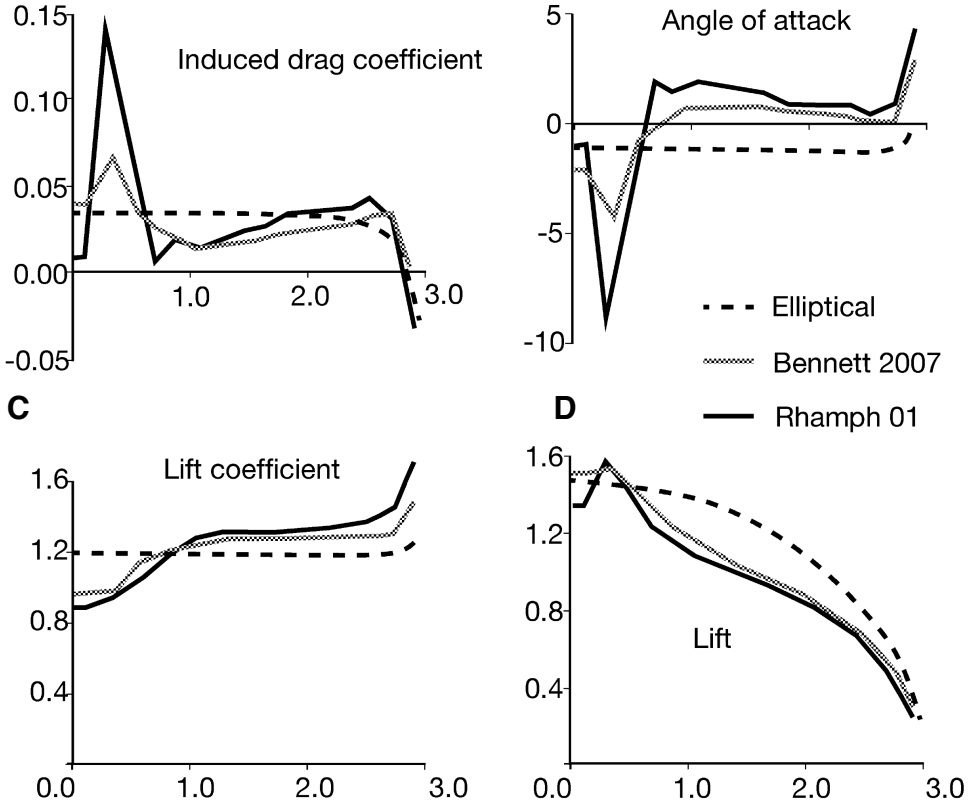

shapes (Bennett (2007) *Pteranodon* and Witton (2007) *Rhamphorhynchus*) are compared with an "ideal" elliptical shape.

Figure 7.11

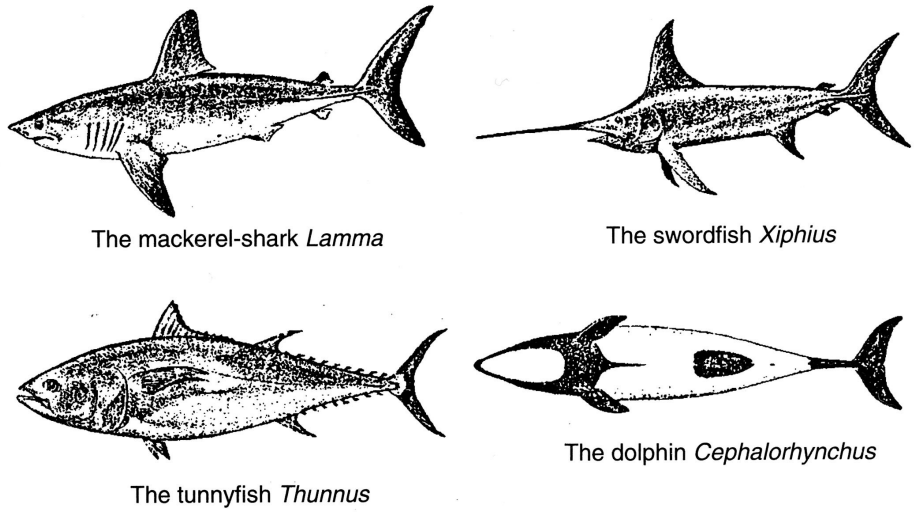

Lunate fin morphology in fish and cetaceans. (From Van Dam 1986).

Figure 7.12

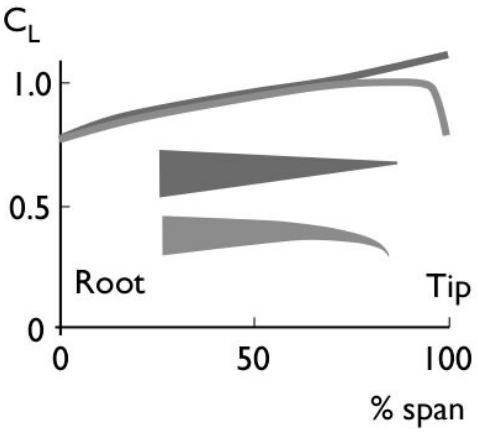

Effect of planform shape on spanwise variation of lift coefficient. Comparison between straight, highly tapered and tapered lunate forms.

Figure 7.13

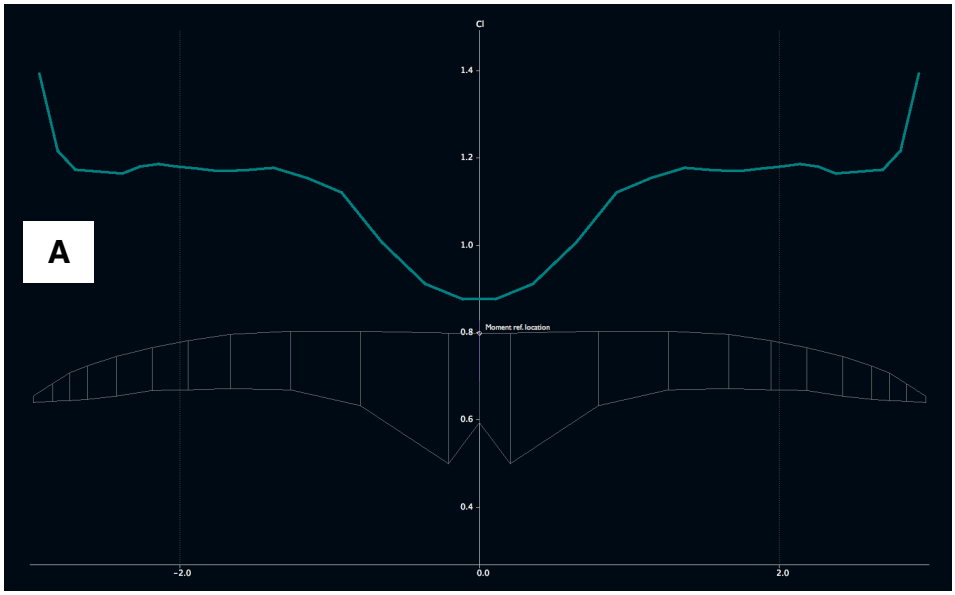

Variation of spanwise lift coefficient, standard (Bennett 2007) wing morphology.

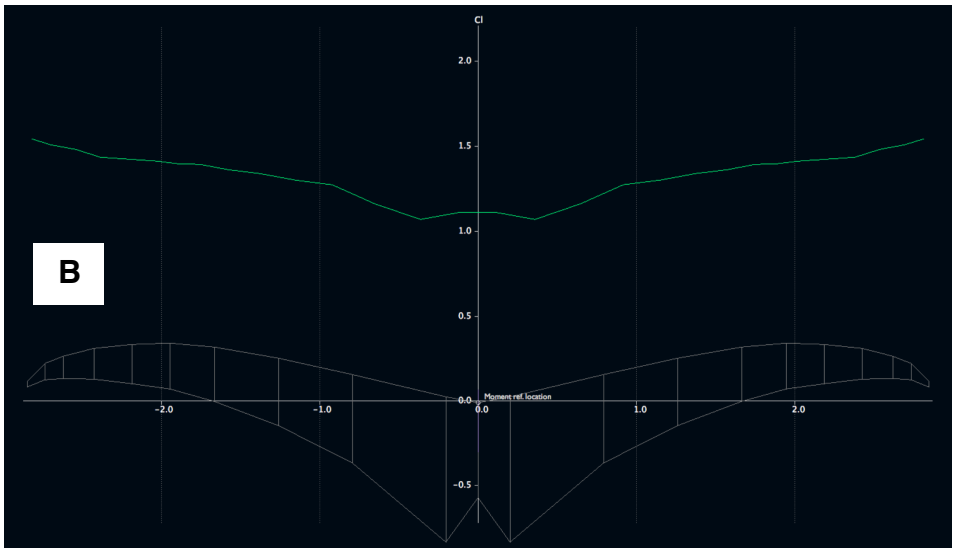

Variation of spanwise lift coefficient (Bennett 2007) wing morphology modified with forward weep and modest tip curvature to give lunate wing tip.

Figure 7.14

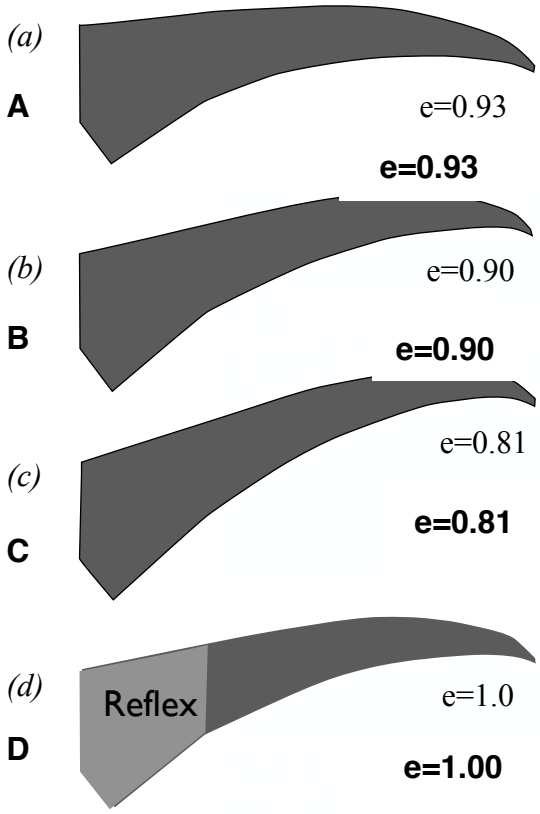

Comparison of the aerodynamic efficiency (as quantified by span efficiency e for a family of wing geometries. In (A) to (C) wings have constant sections, but increasing anterior sweep. The span efficiency is reduced with increases in anterior sweep., (D) has the same planform as (B) but different, reflexed wing sections in the proximal region. The span efficiency is increased significantly and is the highest of all the variants.

Figure 7.15

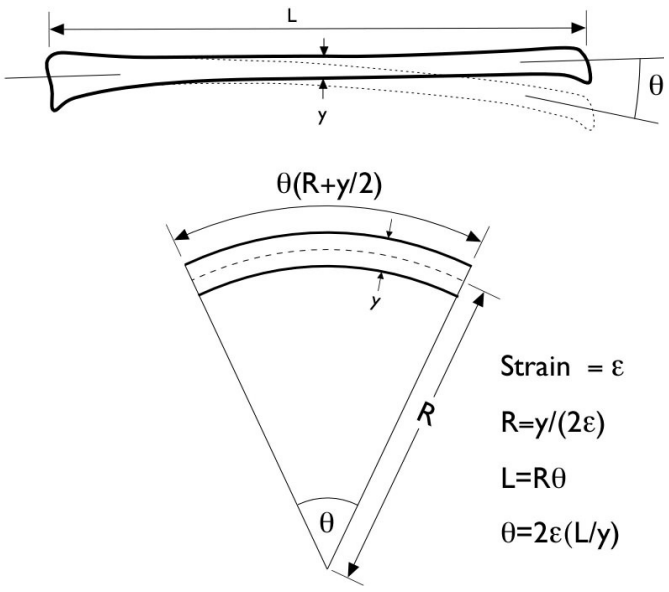

Calculation of wing bone deflection using limiting strain. When a structural section is subjected to a bending load, it deflects, resulting in tensile strain on one face and compressive strain on the other. The radius of curvature (R) is a function of the strain (ε) and using this geometry it is possible to determine the deflection angle (θ) and thus total deflection.

Figure 7.16

Wing bone reconstruction taking account of bone-bending deflection and possible joint flexion (reconstructed from Bennett (2000)). (A) Maximum deflected shape (in response to membrane in

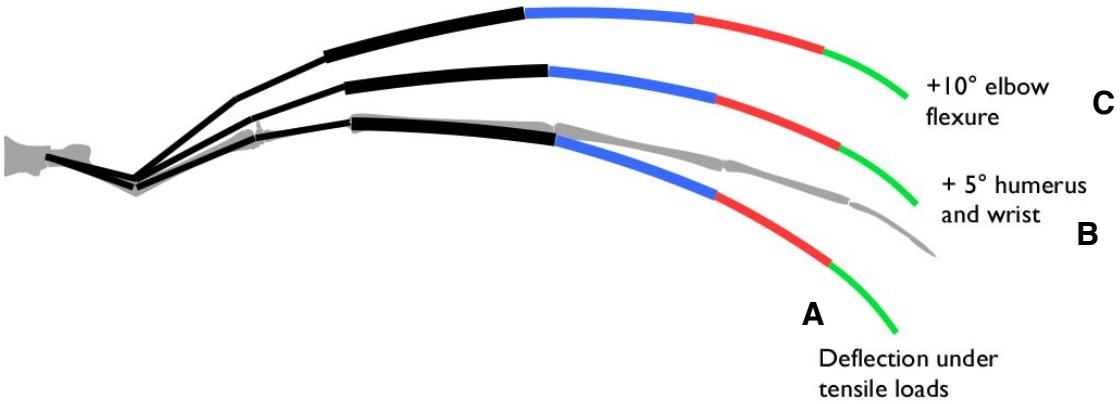

plane tension loading) of wing bones retaining joint angles as reconstructed in Bennett (2000). (B) Effect of 5° humerus and wrist flexion. (C) As in (B), but with additional 10° flexion of the elbow. This wing bone geometry allows the wing shape to be aerodynamically balanced.

Figure 7.17

Effect of wing washout (distal twist) on movement of centre of pressure with change in lift coefficient. With no washout, the centre of pressure moves forwards as lift increases, leading to pitch instability.

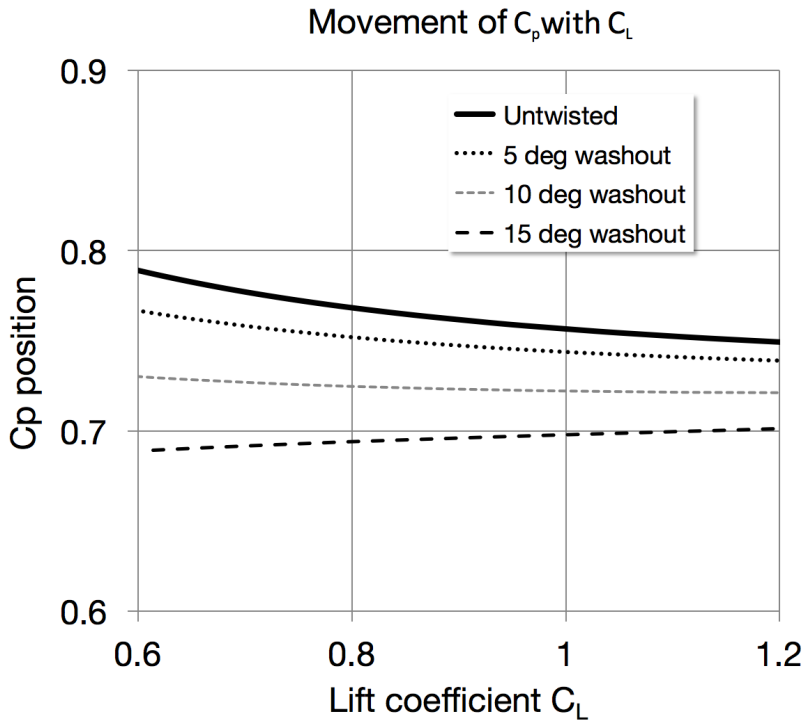

To control this effect it is necessary to twist the wing by 15 degrees in the distal region.

Figure 7.18

Variation of span efficiency with washout angle. As twist increases the span efficiency decreases, resulting in an increase in induced drag. At 15 degrees washout (the amount required for pitch

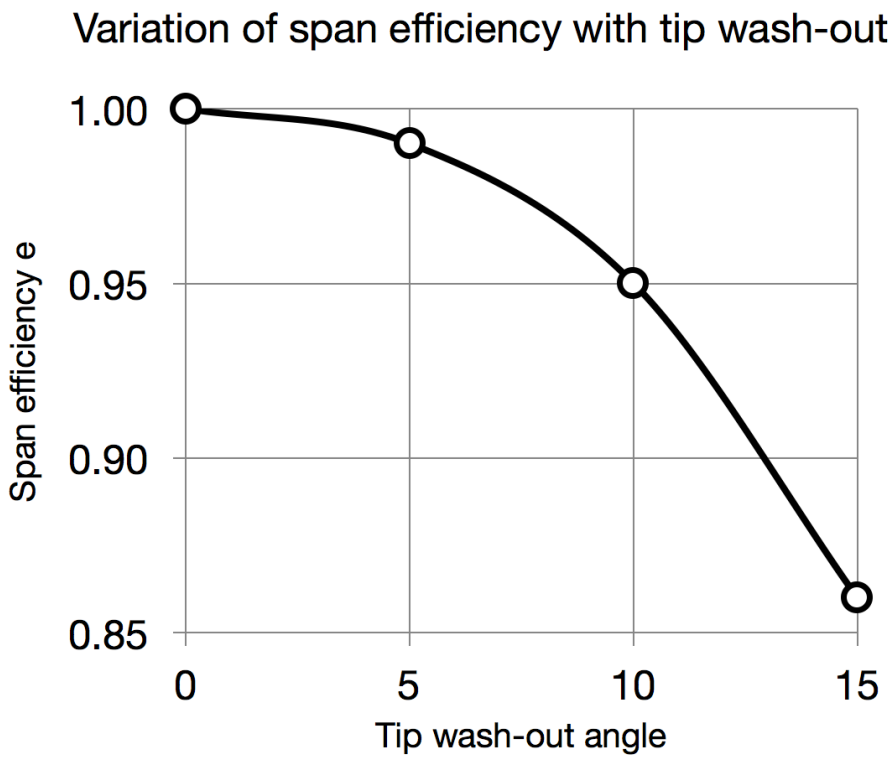

stability) the span efficiency drops to 85%, resulting in a 15% increase in induced drag.

Figure 7.19

Effect of wing flexibility on pitch stability response. The graphs show the movement of the CP with

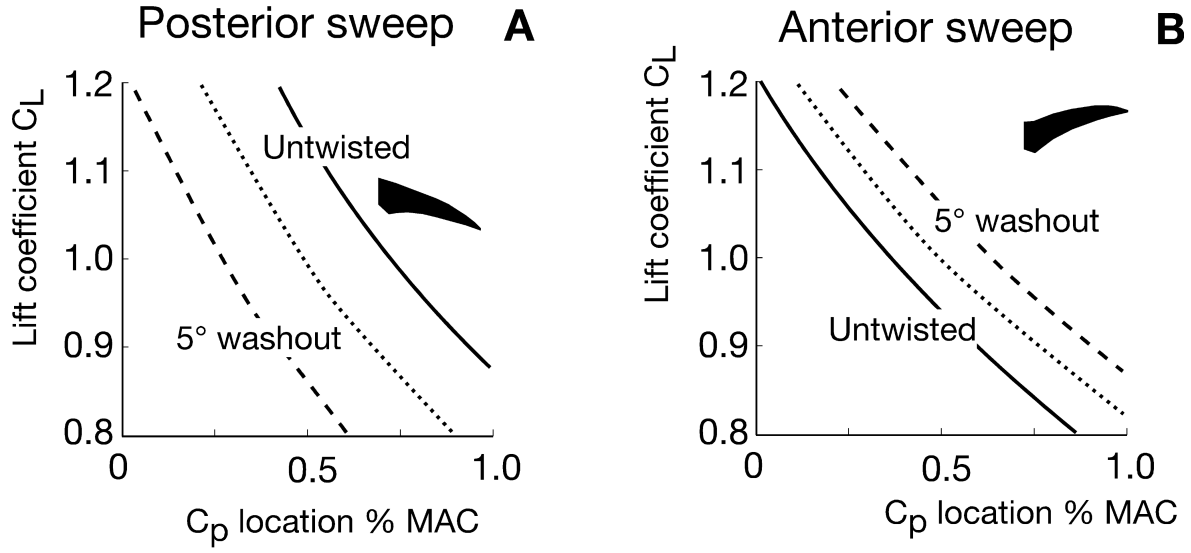

changes in lift coefficient. The solid line is for an untwisted wing and the dashed lines for increasing amounts of washout (the natural deflection under transient aerodynamic load). (A): the effect for a wing with posterior sweep - the centre of pressure moves forwards (the destabilising direction) with increasing twist. In (B) the opposite effect is seen to occur for anterior sweep.

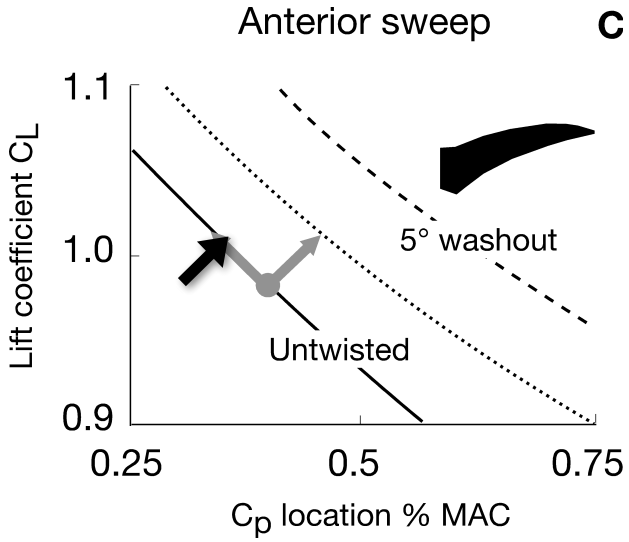

(C) Effect of centre of pressure movement with anterior sweep. When a rigid wing (untwisted) experiences a transient increase in lift (i.e. encountering a gust), the CP moves anteriorly (grey arrow), resulting in pitch instability. However, if the wing flexes in response to this change in loading, the locus of the CP may be along the black arrow, resulting in a net posterior movement, which confers pitch stability. The opposite effect occurs with posterior sweep.